A detailed analysis of S3 and S6 fully-focused SAR waveforms: **Enabling SAMOSA-based retracking** *(paper in review)*

Frithjof Ehlers*, Florian Schlembach, Marcel Kleinherenbrink, Cornelis Slobbe

* f.ehlers@tudelft.nl

CITG, TU Delft

Physical and Space Geodesy

TU Delft TUM

Can we use existing retrackers (like SAMOSA) for FF-SAR waveforms over ocean surfaces?

Goals:

- profiting from increased resolution for clutter removal in the coast
- Consistent observations of SSH, SWH and sigma0
- …

Possible advantages:

- Using already established code rather than deriving a waveform model from scratch
- Maybe using established corrections (e.g. alpha LUT, …)
- …

Earlier studies

Egido, Alejandro, and Walter H. F. Smith. "Fully Focused SAR Altimetry: Theory and Applications." IEEE Transactions on Geoscience and Remote Sensing 55, no. 1 (January 2017): 392–406. https://doi.org/10.1109/TGRS.2016.2607122.

Authors stress that the waveform models ought to be quite similar, suggesting the zero-Doppler beam model for CS2, but considering only an approximate PTR (main lobe).

Rieu, P, T Moreau, L Amarouche, P Thibaut, F Boy, F Borde, and C Mavrocordatos. "From Unfocused to Fully- Focused SAR Processing : Benefits for Different Surfaces," 2018, 20.

On the contrary, authors results suggest that UF-SAR and FF-SAR waveforms look very much alike for S3.

Buchhaupt, Christopher, Luciana Fenoglio, Matthias Becker, and Jürgen Kusche. "Impact of Vertical Water Particle Motions on Focused SAR Altimetry." Advances in Space Research 68, no. 2 (July 2021): 853–74. https://doi.org/10.1016/j.asr.2020.07.015.

Authors derive a full (and complex) model for the CS2 FF-SAR delay-Doppler map in the spectral domain and in presence of sea surface motion, but without validation on measured data.

Earlier studies

Egido, Alejandro, and Walter H. F. Smith. "Fully Focused SAR Altimetry: Theory and Applications." IEEE Transactions on Geoscience and Remote Sensing 55, no. 1 (January 2017): 392–406. https://doi.org/10.1109/TGRS.2016.2607122.

Authors stress that the waveform models ought to be quite similar, suggesting the zero-Doppler beam model for CS2, but considering only an approximate PTR (main lobe).

Rieu, P, T Moreau, L Amarouche, P Thibaut, F Boy, F Borde, and C Mavrocordatos. "From Unfocused to Fully- Focused SAR Processing : Benefits for Different Surfaces," 2018, 20.

On the contrary, authors results suggest that UF-SAR and FF-SAR waveforms look very much alike for S3.

Buchhaupt, Christopher, Luciana Fenoglio, Matthias Becker, and Jürgen Kusche. "Impact of Vertical Water Particle Motions on Focused SAR Altimetry." Advances in Space Research 68, no. 2 (July 2021): 853–74. https://doi.org/10.1016/j.asr.2020.07.015.

Authors derive a full (and complex) model for the CS2 FF-SAR delay-Doppler map in the spectral domain and in presence of sea surface motion, but without validation on measured data.

Emulated UF-SAR processing like in:
Egido, Alejandro, Salvatore Dinardo, and Christopher Ray. "The Case for Increasing the Posting Rate in Delay/Doppler Altimeters." Advances in Space Research 68, no. 2 (July 2021): 930–36. https://doi.org/10.1016/j.asr.2020.03.014.

UF-SAR and FF-SAR waveform comparisons

S3
SWH ~ 1.5 m

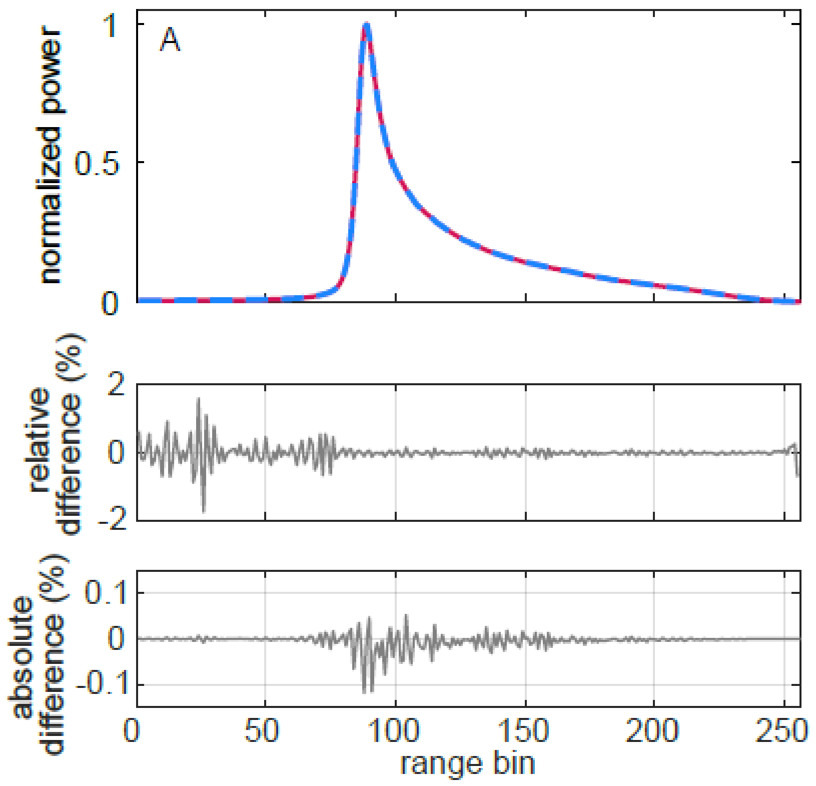

relative difference: 100·(UF-SAR - FF-SAR)/FF-SAR [%]
absolute difference: 100·(UF-SAR - FF-SAR) [%]

UF-SAR and FF-SAR waveform comparisons

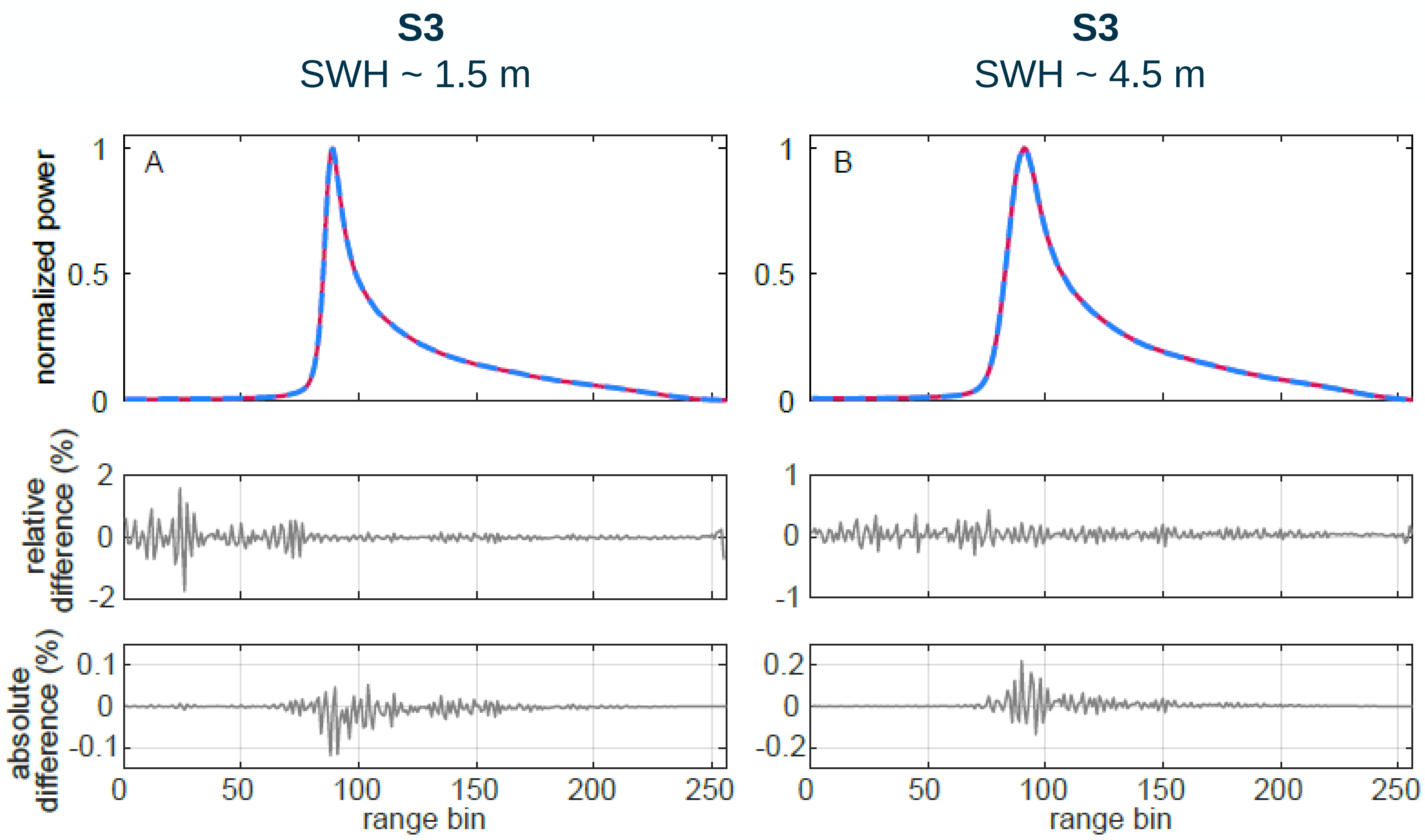

relative difference: 100·(UF-SAR - FF-SAR)/FF-SAR [%]
absolute difference: 100·(UF-SAR - FF-SAR) [%]

UF-SAR and FF-SAR waveform comparisons

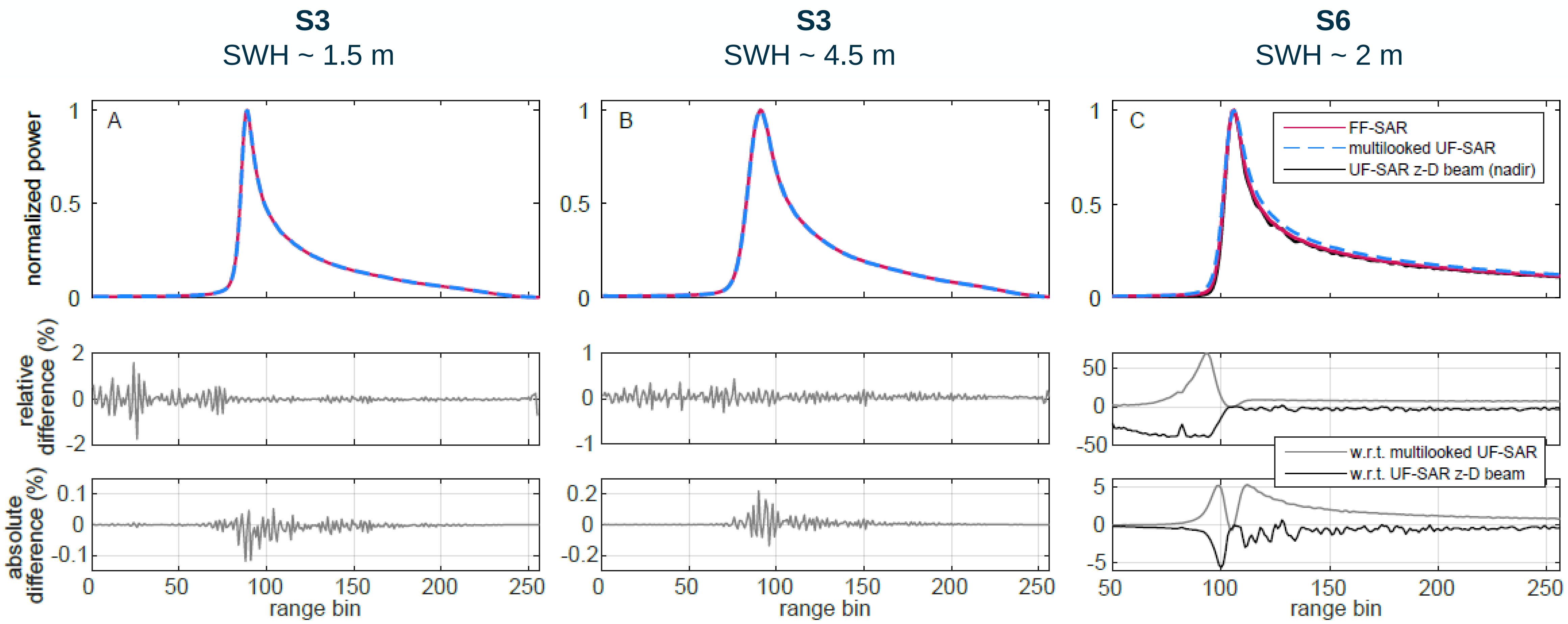

relative difference: $100 \cdot (\text{UF-SAR} - \text{FF-SAR})/\text{FF-SAR}$ [%]

absolute difference: $100 \cdot (\text{UF-SAR} - \text{FF-SAR})$ [%]

Waveform model (static case)

Can be obtained from triple convolution of

- Sea surface elevation probability density, p(z)
- Flat Surface Impulse Response (FSIR, illumination geometry, antenna pattern, surface properties, …)
- System point target response / impulse response function (IRF)

See e.g. Brown et al. 1977; Ray et al. 2015.

Waveform model (static case)

Can be obtained from triple convolution of

- Sea surface elevation probability density, p(z) — same for UF-SAR and FF-SAR
- Flat Surface Impulse Response (FSIR, illumination geometry, antenna pattern, surface properties, …) — same for UF-SAR and FF-SAR
- System point target response / impulse response function (IRF)

See e.g. Brown et al. 1977; Ray et al. 2015.

Waveform model (static case)

Can be obtained from triple convolution of

- Sea surface elevation probability density, p(z) — same for UF-SAR and FF-SAR
- Flat Surface Impulse Response (FSIR, illumination geometry, antenna pattern, surface properties, …) — same for UF-SAR and FF-SAR
- System point target response / impulse response function (IRF) — different for UF-SAR and FF-SAR

See e.g. Brown et al. 1977; Ray et al. 2015.

Some simplifications

The waveform model can be rewritten with the “transponder image”.

For multilooked UF-SAR, this is the sum of the IRF of all Doppler beams (multilooked IRF). For FF-SAR it is the IRF.

$$\overbrace{C \int \mathrm{dz}\; p(z) \int \mathrm{dy} \int \mathrm{dx}\; \frac{G^2(x,y)\sigma_0(x,y)}{r^4} h^2(r - R(x,y,z), x)}^{\text{waveform integral}}$$

x: along-track distance
z: cross-track distance
z: elevation

Some simplifications

The waveform model can be rewritten with the "transponder image" – the radargram as observed over a point target.

For multilooked UF-SAR, this is the sum of the IRF of all Doppler beams (multilooked IRF). For FF-SAR it is the IRF.

$$\overbrace{C \int \mathrm{dz}\, p(z) \int \mathrm{dy} \int \mathrm{dx}\, \frac{G^2(x,y)\sigma_0(x,y)}{r^4} h^2(r - R(x,y,z), x)}^{\text{waveform integral}} \approx \overbrace{C \int \mathrm{dz}\, p(z) \int \mathrm{dy}\, G_y^2(y)}^{\text{same for UF-SAR \& FF-SAR}} \underbrace{\int \mathrm{dx}}_{\text{along-track integral}} \overbrace{\mathcal{T}(r - r_0(y,z), x)}^{\text{"transponder image"}}$$

x: along-track distance
z: cross-track distance
z: elevation

Some simplifications

The waveform model can be rewritten with the "transponder image" – the radargram as observed over a point target.

For multilooked UF-SAR, this is the sum of the IRF of all Doppler beams (multilooked IRF). For FF-SAR it is the IRF.

$$\overbrace{C\int \mathrm{dz}\; p(z)\int \mathrm{dy} \int \mathrm{dx}\; \frac{G^2(x,y)\sigma_0(x,y)}{r^4}\, h^2(r-R(x,y,z),x)}^{\text{waveform integral}}$$

$$\approx \overbrace{C\int \mathrm{dz}\; p(z)\int \mathrm{dy}\; G_y^2(y)}^{\text{same for UF-SAR \& FF-SAR}}\; \boxed{\underbrace{\int}_{\text{along-track integral}} \mathrm{dx}\; \overbrace{\mathcal{T}\,(r-r_0(y,z),x)}^{\text{"transponder image"}}}$$

x: along-track distance
z: cross-track distance
z: elevation

Transponder images - S3

$$\int \mathrm{d}x\, \mathcal{T}\,(r - r_0(y,z), x)$$

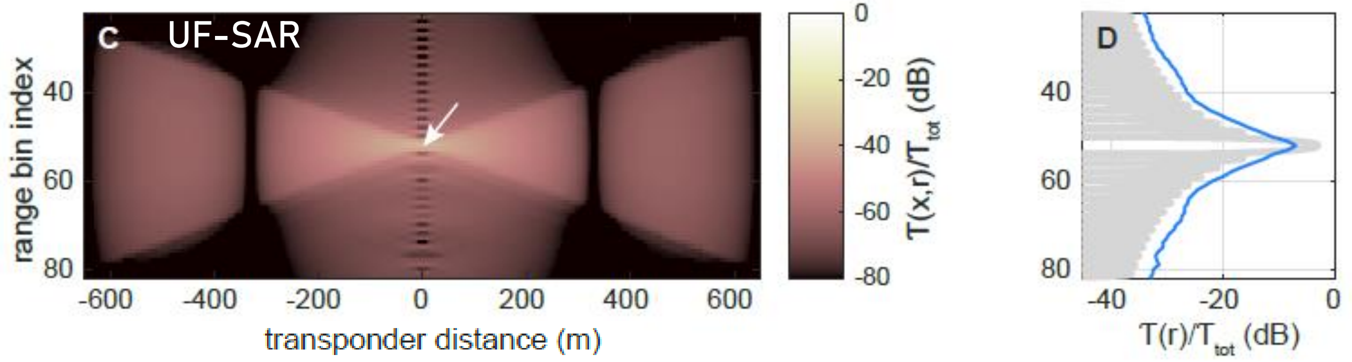

Transponder images - S3

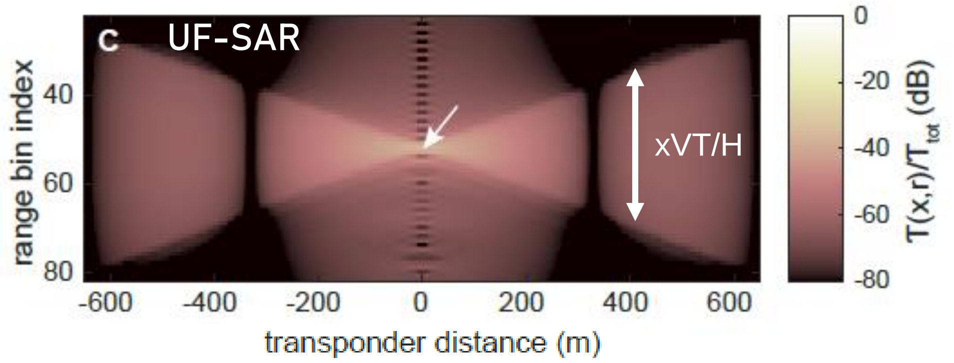

$$\int \mathrm{dx}\, \mathcal{T}\,(r - r_0(y,z), x)$$

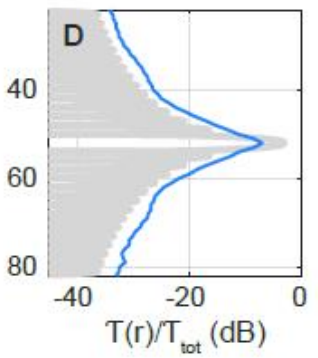

Transponder images - S3

$$\int dx\, \mathcal{T}\,(r - r_0(y,z), x)$$

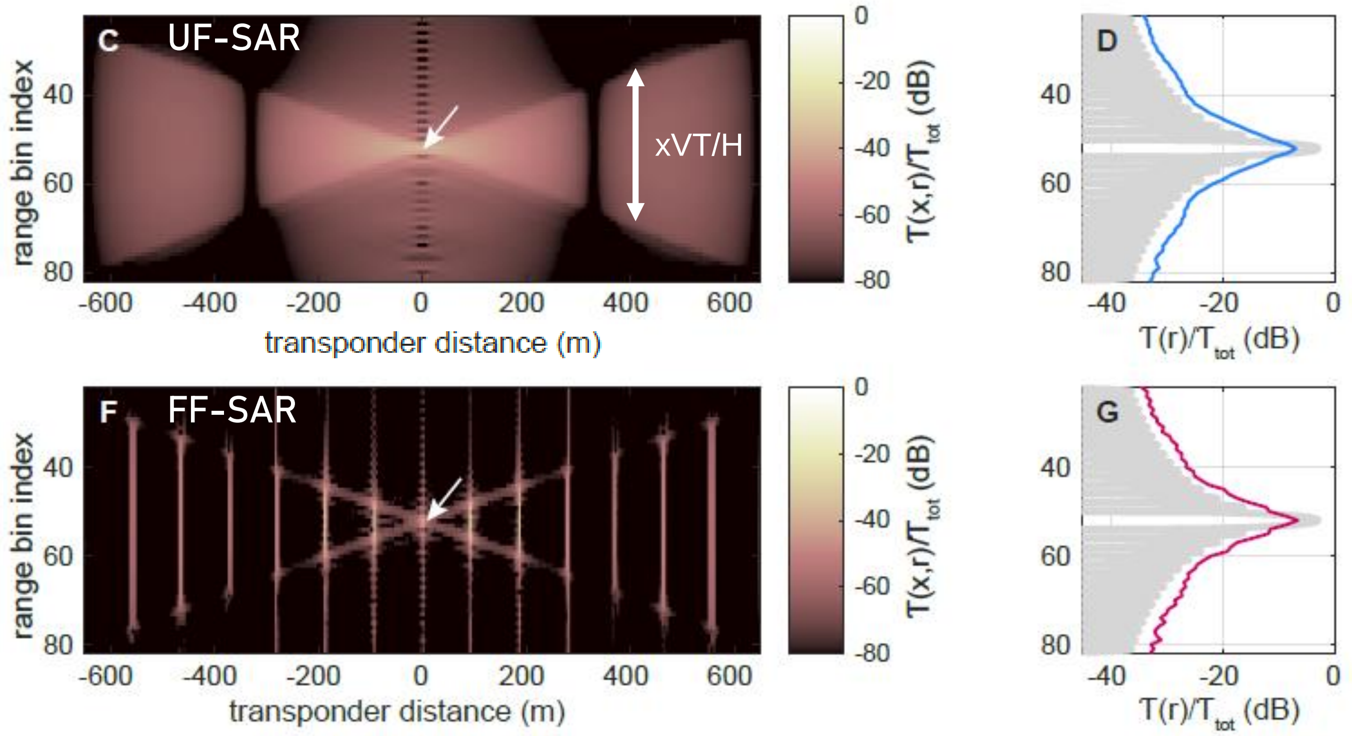

The along-track integrals of the transponder images look very similar for UF-SAR and FF-SAR

Transponder images – S6

$$\int dx\, \mathcal{T}\,(r - r_0(y,z), x)$$

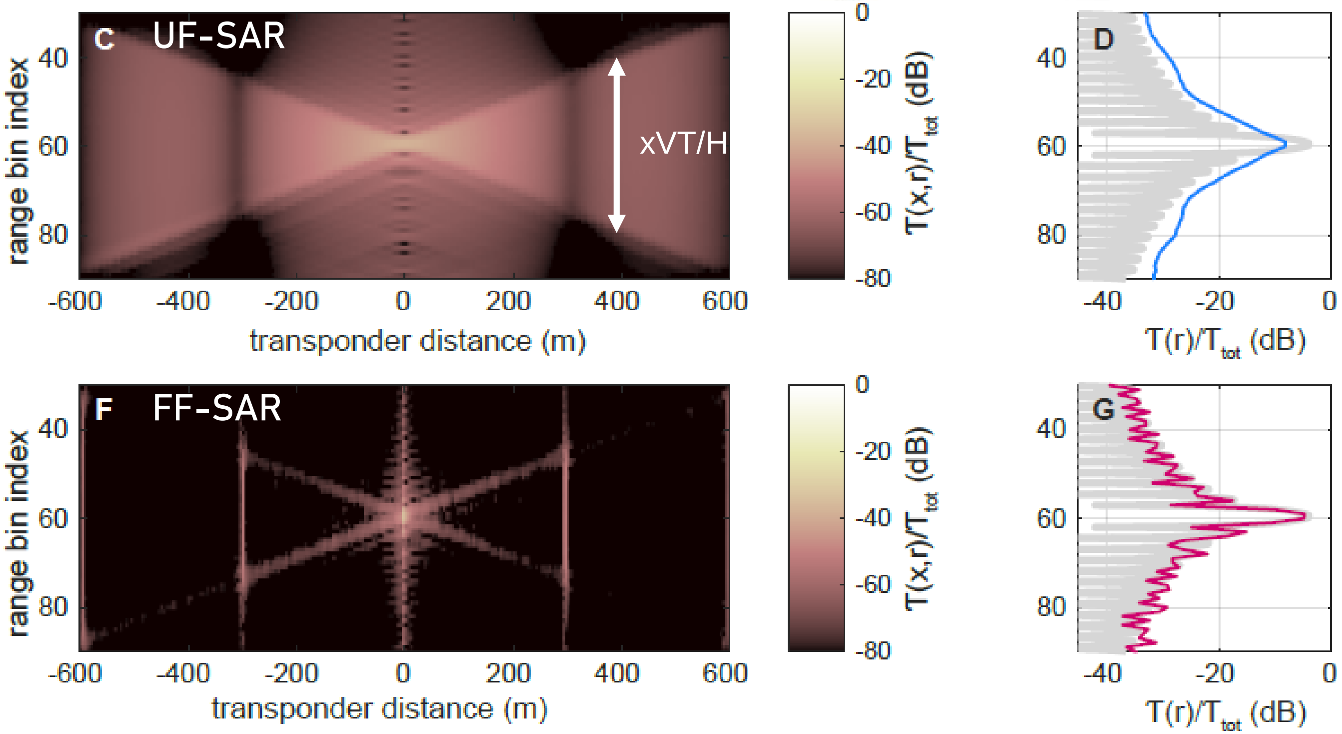

The along-track integral of the FF-SAR transponder image is much sharper!

Transponder images - S3

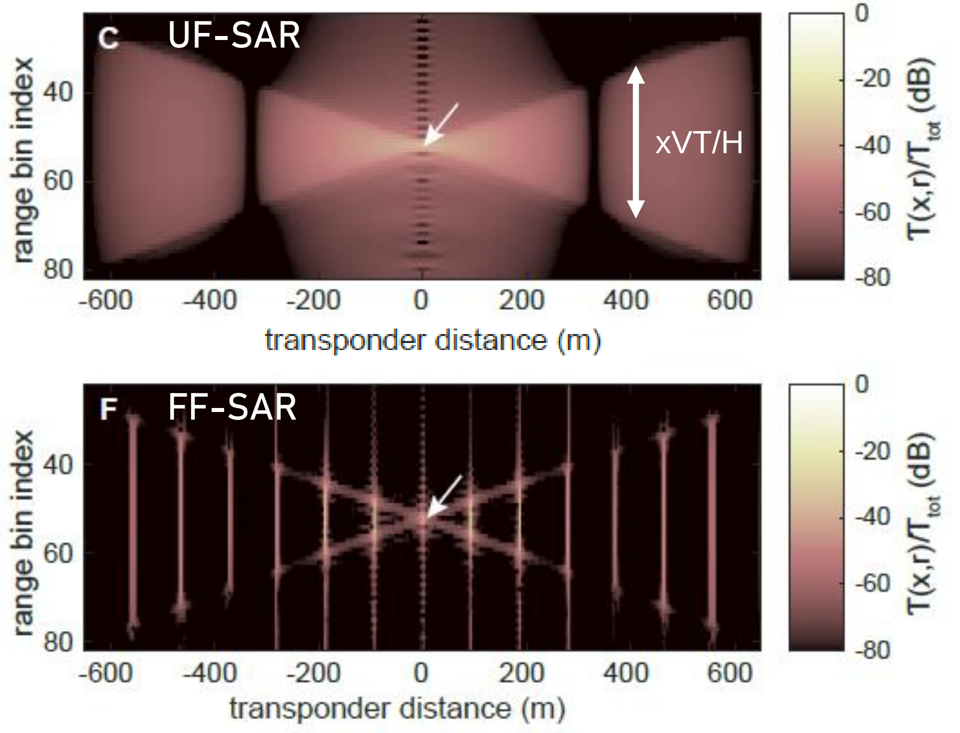

$$\int dx\, \mathcal{T}\left(r - r_0(y,z), x\right)$$

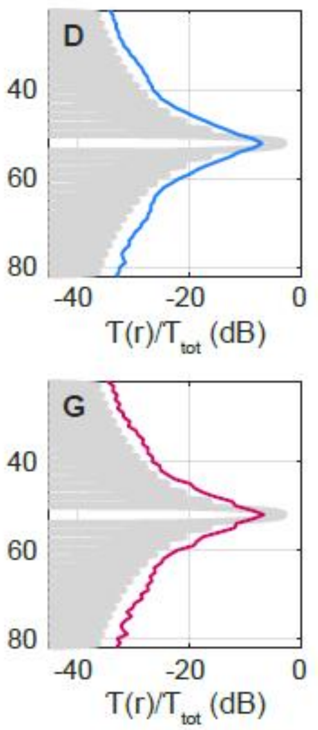

The along-track integrals of the transponder images look very similar for UF-SAR and FF-SAR

Transponder images - S3

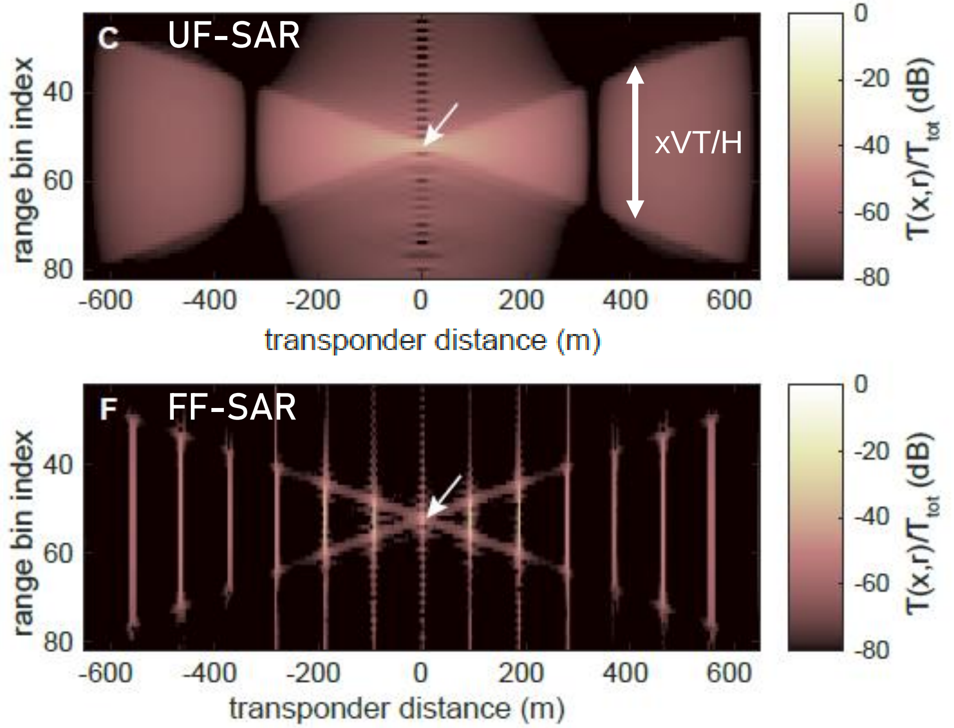

$$\int dx\, \mathcal{T}\left(r - r_0(y,z), x\right)$$

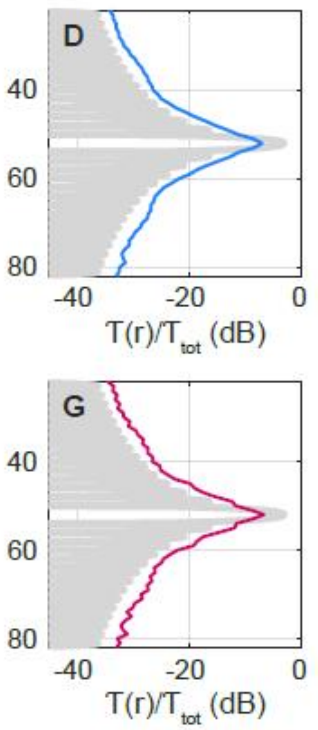

The along-track integrals of the transponder images look very similar for UF-SAR and FF-SAR

main lobe

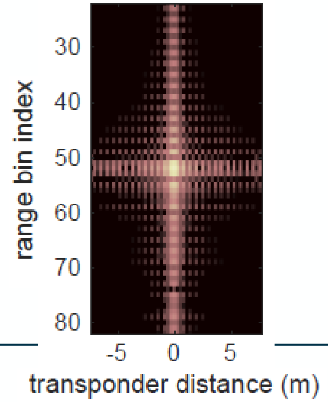

Transponder images - S3

$$\int dx\, \mathcal{T}\,(r - r_0(y,z), x)$$

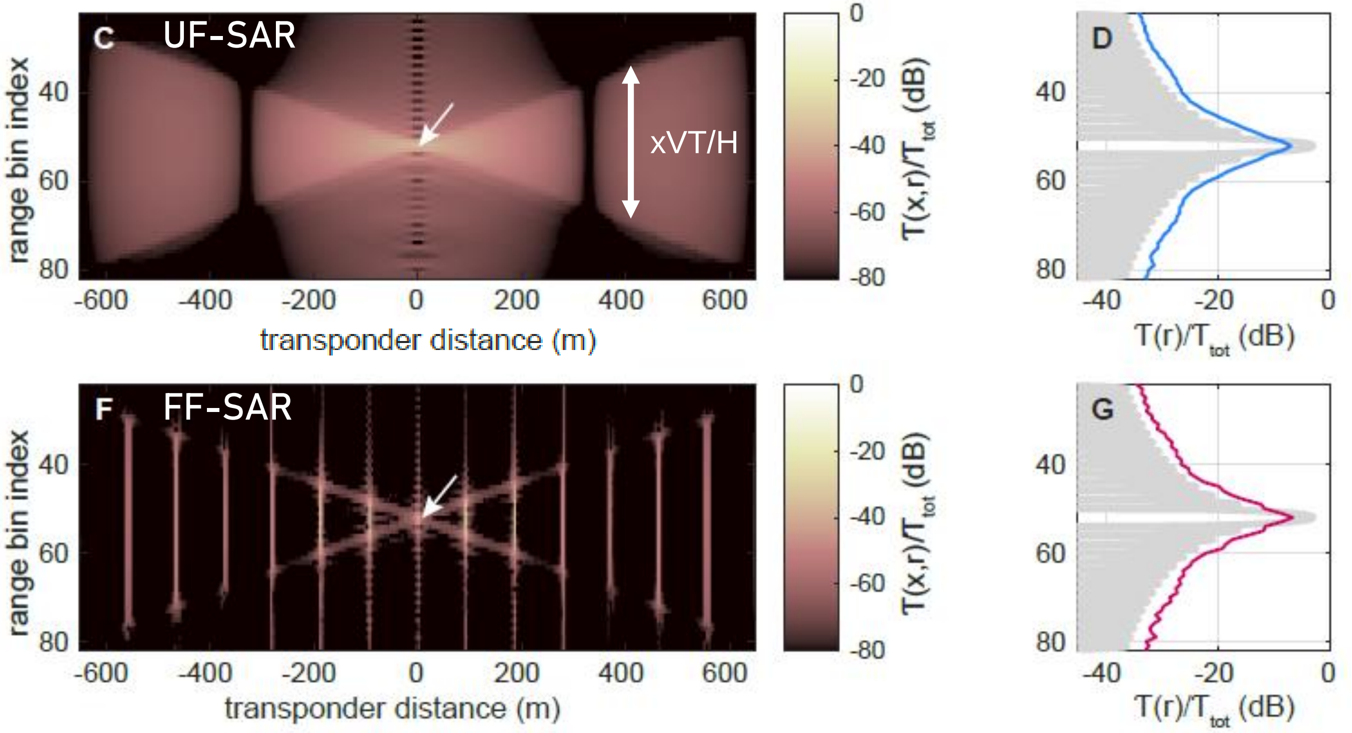

The along-track integrals of the transponder images look very similar for UF-SAR and FF-SAR

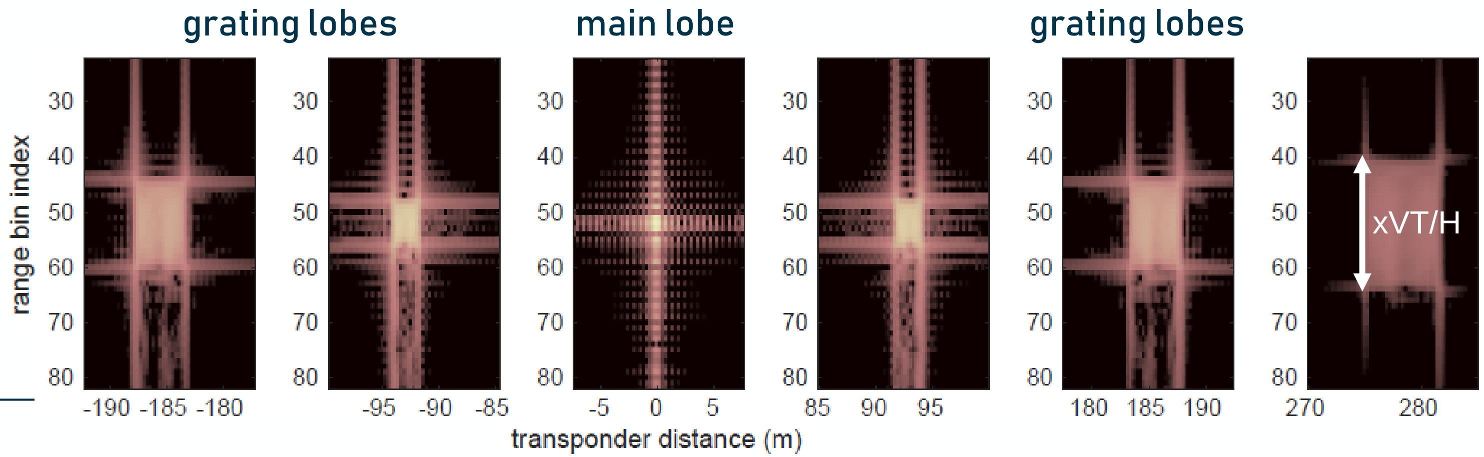

The blurring of the FF-SAR grating lobes has huge influence on the waveform and is not described in the IRF approximations [Egido et al. (2017); Guccione et al. (2018)]

Only the blurring in range will have noticeable influence on the waveform.

Modelled transponder images

Accounting only for the blur in range, we find a relatively simple way of rewriting the FF-SAR IRF, which reproduces the behavior observed before.

$$\boxed{\begin{aligned}\mathcal{T}_{\mathrm{FF}}(r-r_0,x) &= h_{\mathrm{FF}}^2(x)\sum_{t_p} G_x^2(Vt_p+x) \\ &\mathrm{sinc}^2\left[\frac{2B}{c}\left(r-r_0(y,z)-\left(\frac{xV}{H}t_p+\frac{x^2}{2H}-\frac{xf_cV}{Hs}\right)\right)\right]\end{aligned}}$$

Modelled transponder images

Accounting only for the blur in range, we find a relatively simple way of rewriting the FF-SAR IRF, which reproduces the behavior observed before.

$$\mathcal{T}_{\mathrm{FF}}(r - r_0, x) = h^2_{\mathrm{FF}}(x) \sum_{t_p} G^2_x(V t_p + x)$$
$$\mathrm{sinc}^2\left[\frac{2B}{c}\left(r - r_0(y,z) - \left(\frac{xV}{H}t_p + \frac{x^2}{2H} - \frac{x f_c V}{H s}\right)\right)\right]$$

$$\int \mathrm{d}x\, \mathcal{T}\,(r - r_0(y,z), x)$$

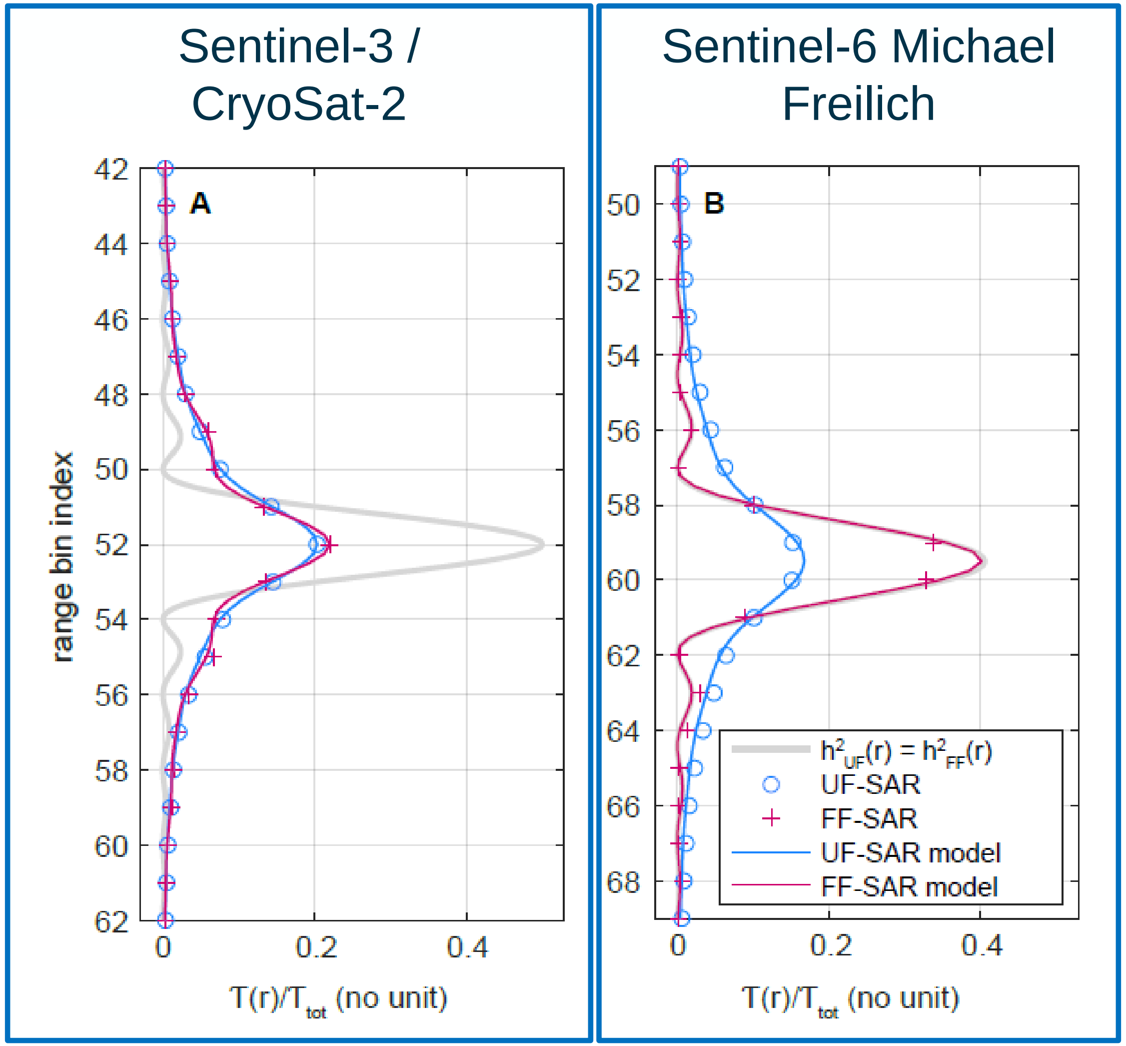

Modelled transponder images

Accounting only for the blur in range, we find a relatively simple way of rewriting the FF-SAR IRF, which reproduces the behavior observed before.

$$\mathcal{T}_{\mathrm{FF}}(r - r_0, x) = h_{\mathrm{FF}}^2(x) \sum_{t_p} G_x^2(V t_p + x)$$
$$\mathrm{sinc}^2\left[\frac{2B}{c}\left(r - r_0(y,z) - \left(\frac{xV}{H} t_p + \frac{x^2}{2H} - \frac{x f_c V}{H s}\right)\right)\right]$$

- So S3 FF-SAR and UF-SAR waveforms closely resemble each other.
- Considering only the S6 FF-SAR main lobe, we can show approximate equality of the waveform with the UF-SAR zero-Doppler beam.

$$\int \mathrm{dx}\, \mathcal{T}\,(r - r_0(y,z), x)$$

Sentinel-3 / CryoSat-2

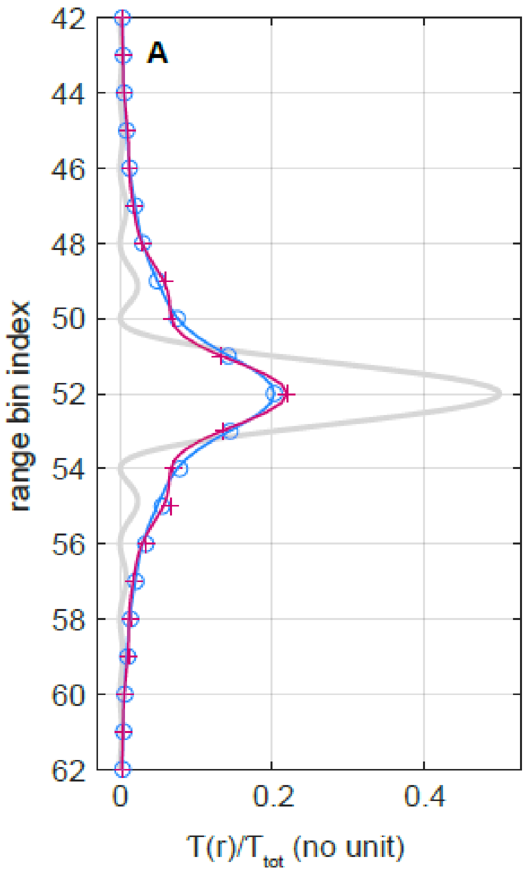

Sentinel-6 Michael Freilich

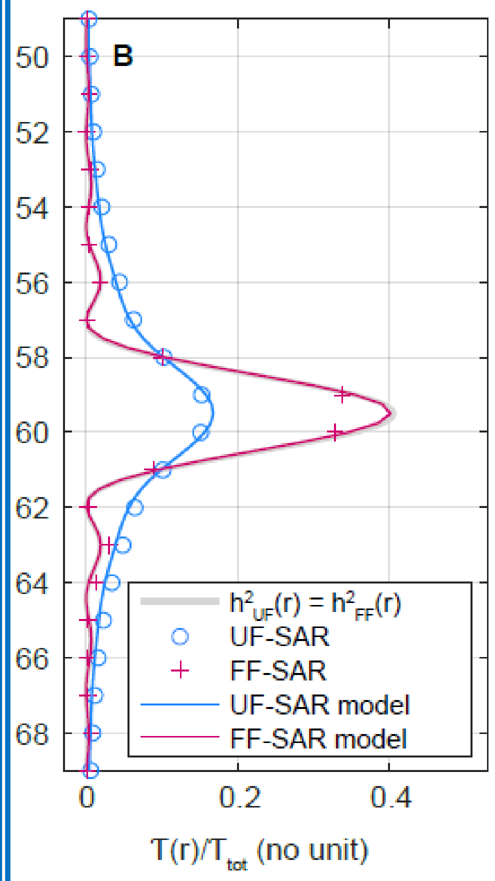

Some retracking results

Sentinel-3

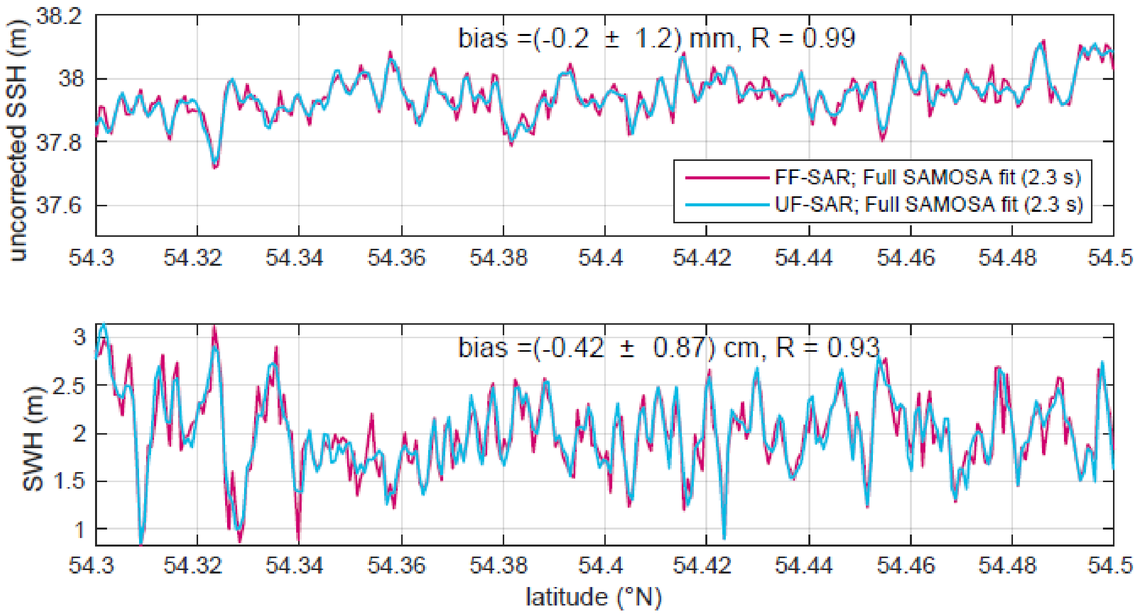

Sentinel-6 Michael Freilich

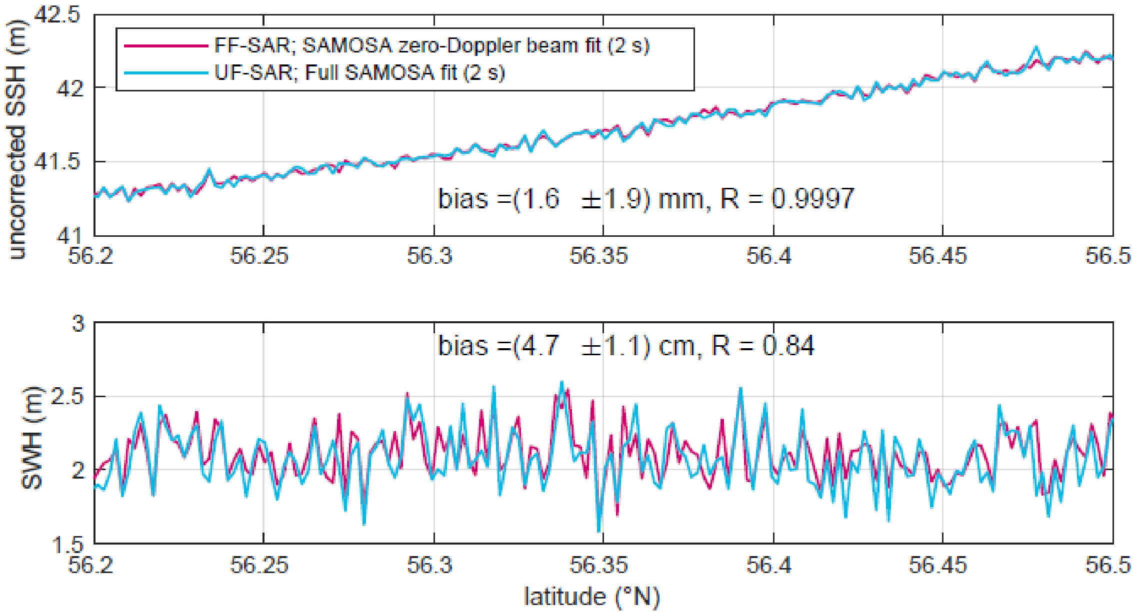

Take home messages

- For Sentinel-3, unfocused and fully-focused SAR waveforms resemble each other (in an average). Hence, the very same waveform model should be used for consistent retracking. The coherent integration time (FF-SAR) determines the amount of Doppler beams (UF-SAR) and vice versa.

- For Sentinel-6, fully focused SAR waveforms better resemble the unfocused SAR zero-Doppler beam. This can be derived explicitly in case of a static sea surface. Hence, e.g. the SAMOSA zero-Doppler beam model is recommended. However, particularly a positive wave height bias remains, which may be due to effects of sea surface motion.

Backup slides

Validation against EUMETSAT L1b

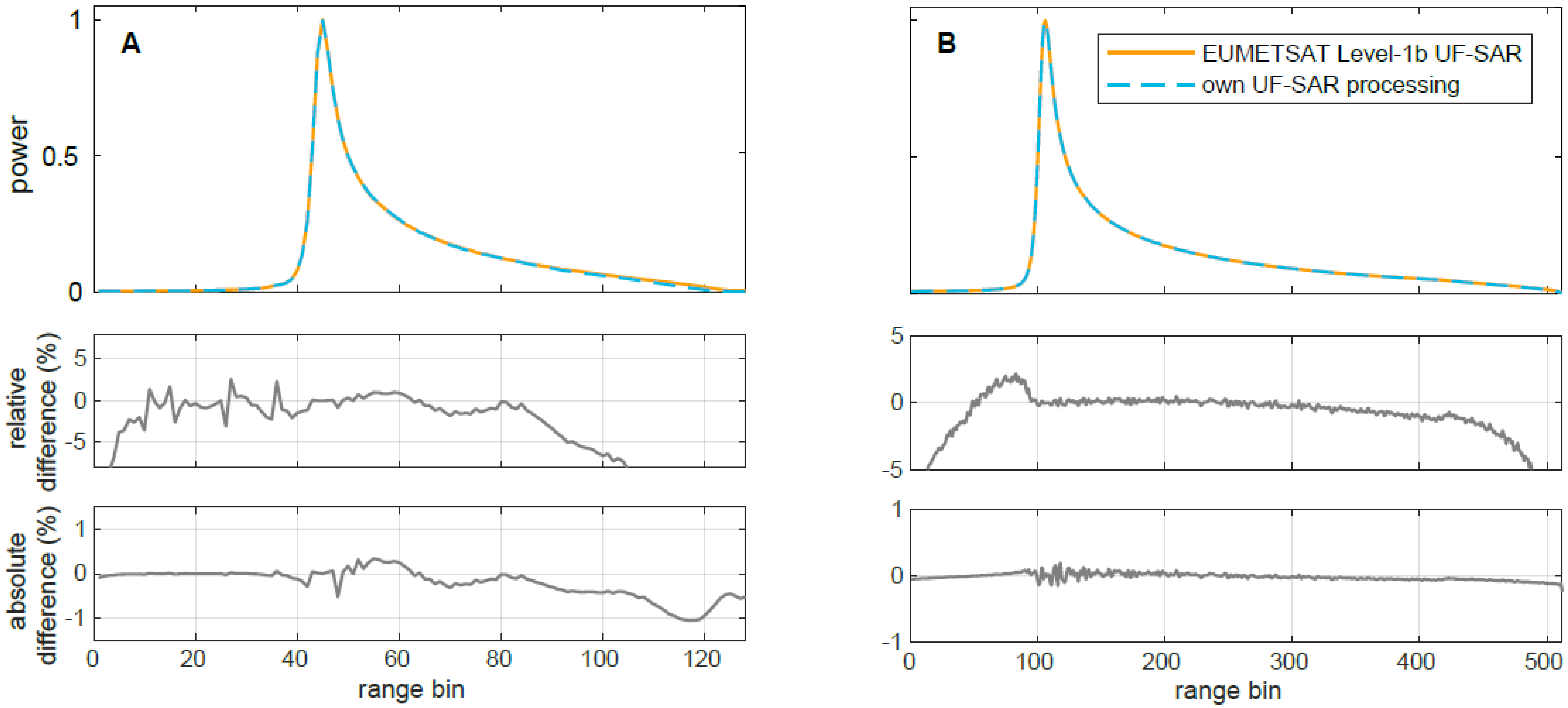

Simultaneous processing of UF-SAR and FF-SAR

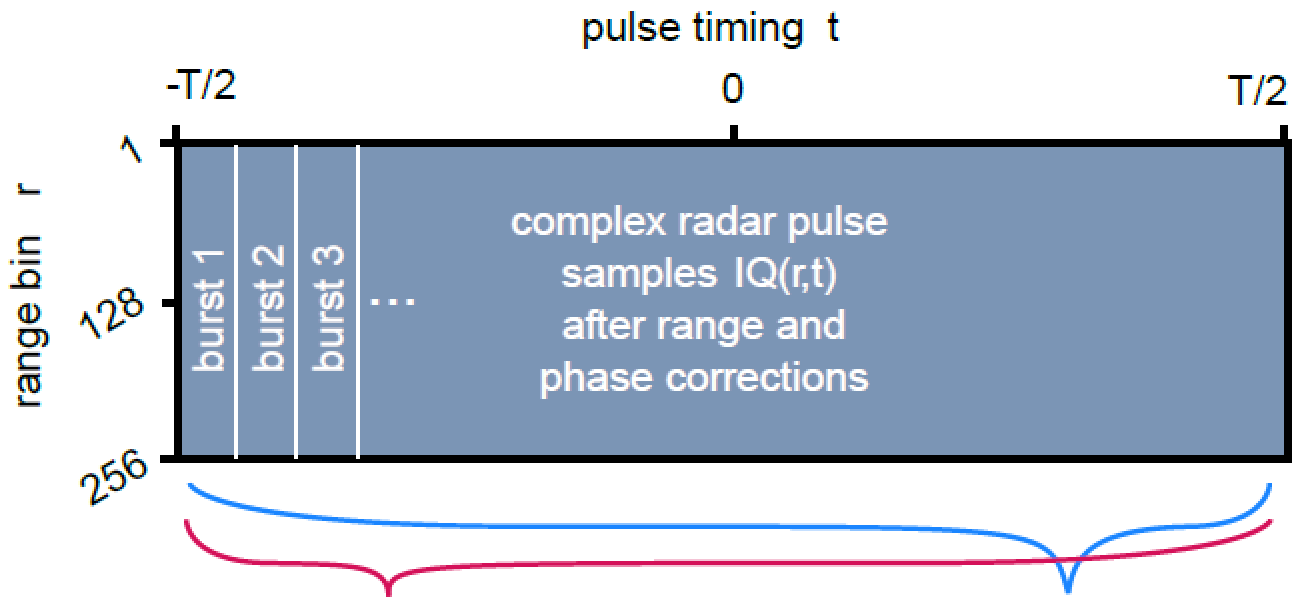

FF-SAR power waveform

$$P(r) = \left| \sum_{\text{all pulses}} IQ(r,t) \right|^2$$

UF-SAR power waveform

$$P(r) = \sum_{\text{bursts}} \left| \sum_{\substack{\text{pulses} \\ \text{within bursts}}} IQ(r,t) \right|^2$$

As in Egido et al. (2021)

Modelled transponder images

Accounting only for the blur in range, we find a relatively simple way of rewriting the FF-SAR IRF, which reproduces the behavior observed before.

$$\mathcal{T}_{\mathrm{FF}}(r-r_0,x) = h_{\mathrm{FF}}^2(x)\sum_{t_p} G_x^2(Vt_p+x)$$
$$\mathrm{sinc}^2\left[\frac{2B}{c}\left(r-r_0(y,z)-\left(\frac{xV}{H}t_p+\frac{x^2}{2H}-\frac{xf_cV}{Hs}\right)\right)\right]$$

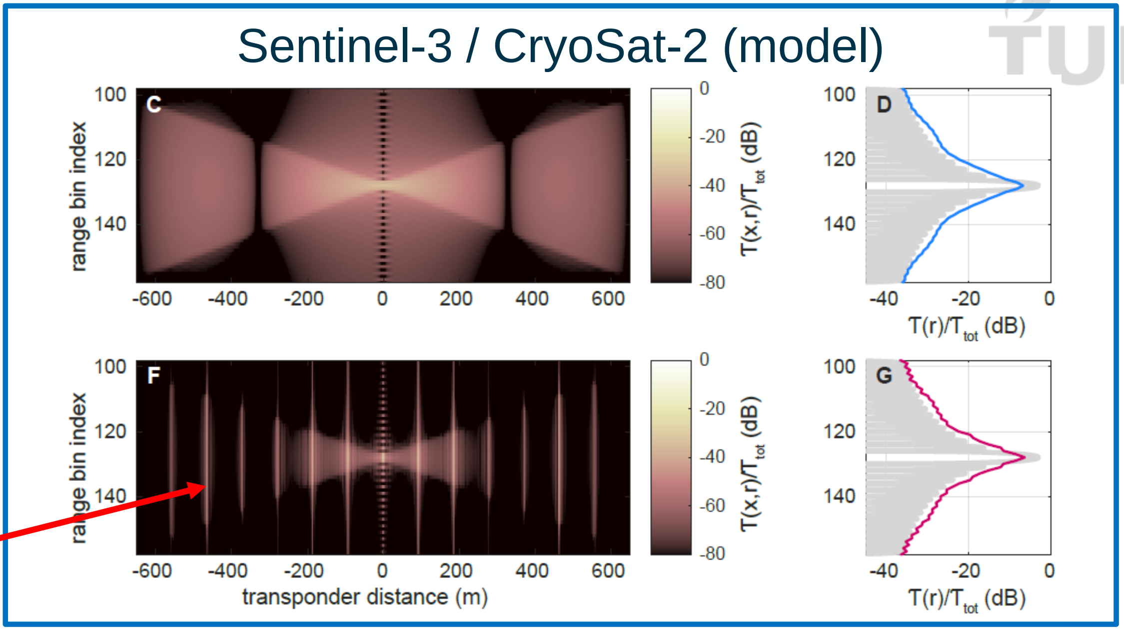

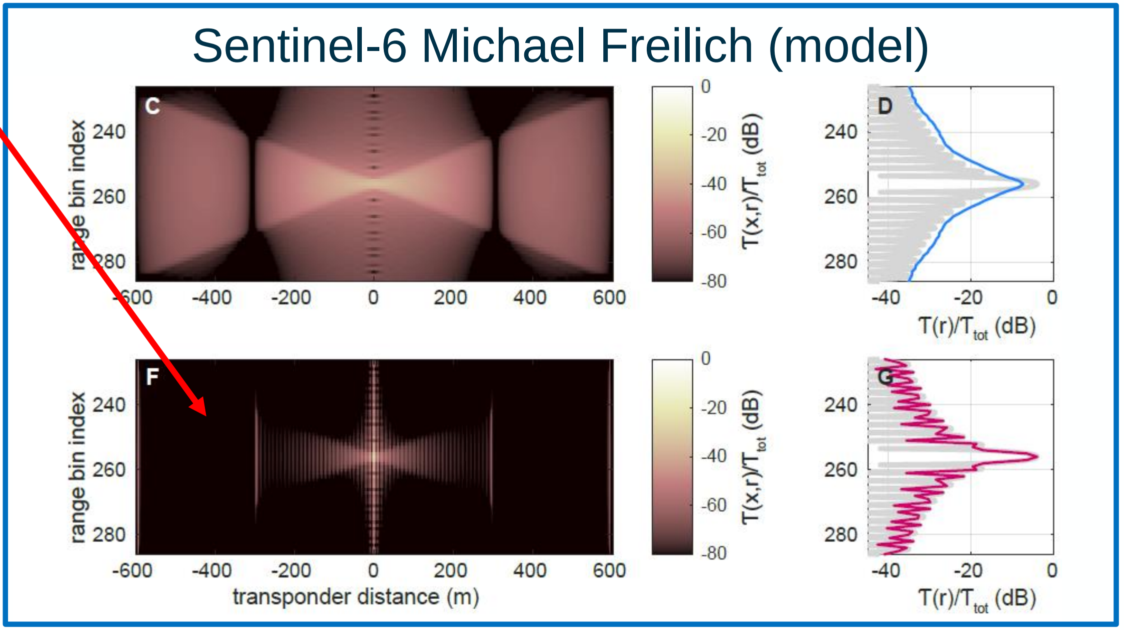

Waveforms

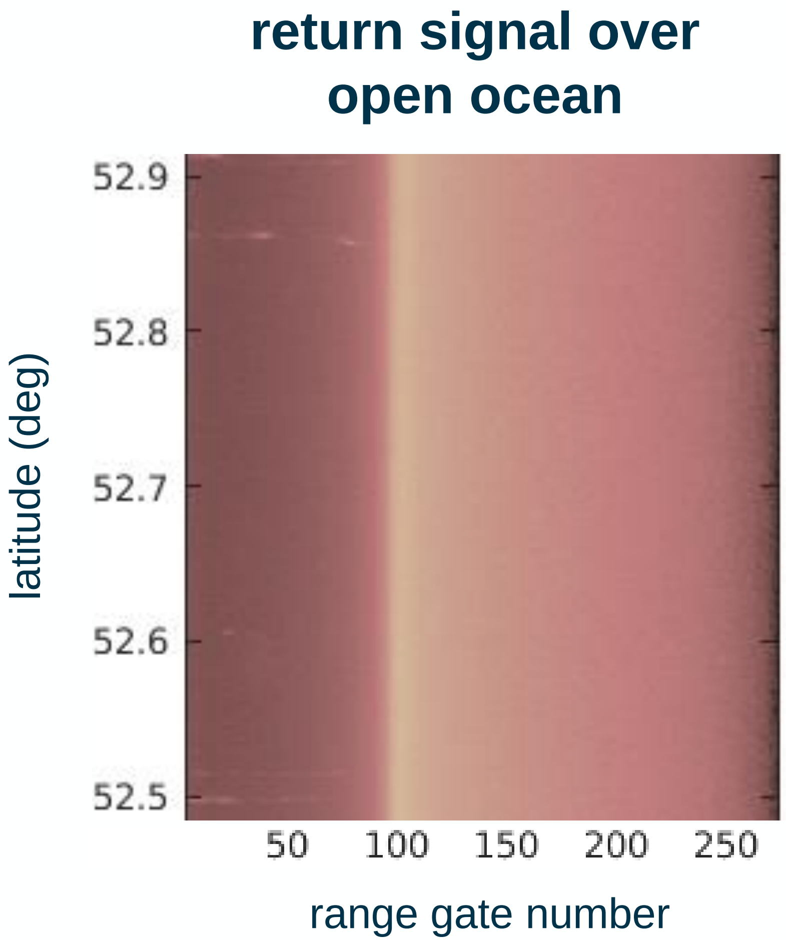
return signal over
open ocean
52.9
52.8
52.7
52.6
52.5
latitude (deg)
50
100
150
200
250
range gate number

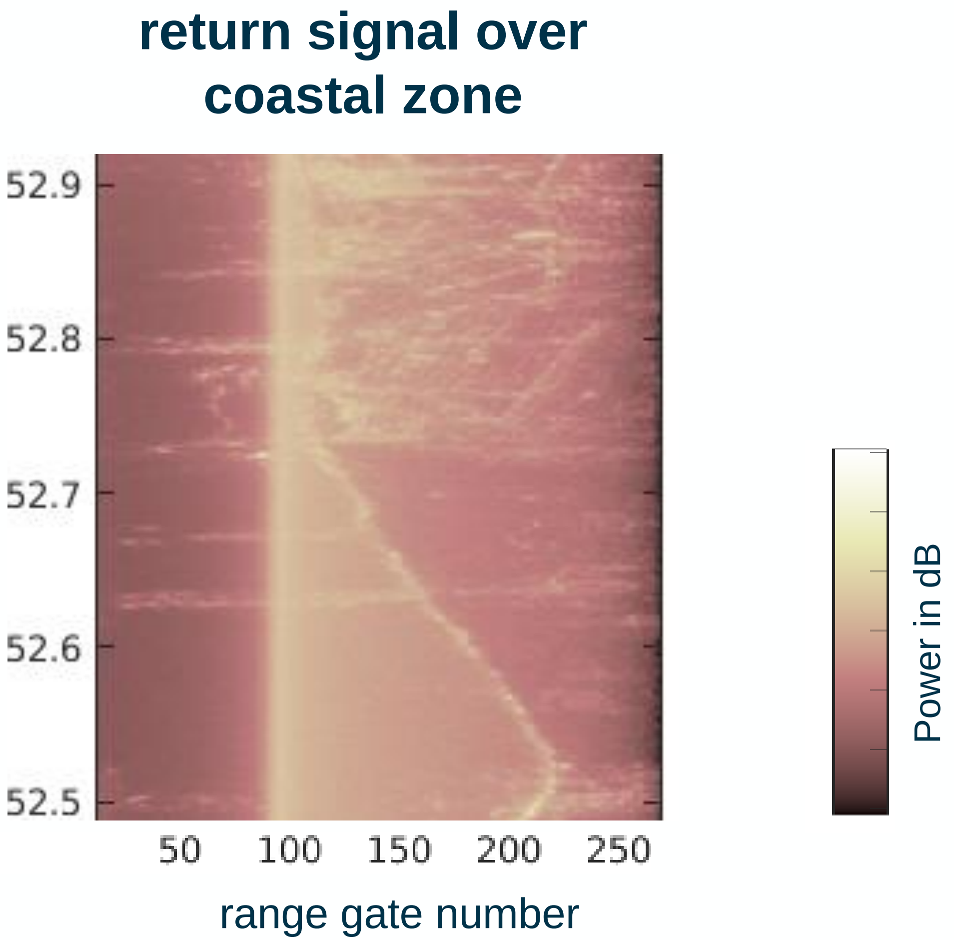
return signal over
coastal zone
52.9
52.8
52.7
52.6
52.5
50
100
150
200
250
range gate number
Power in dB

Closed-burst and open-burst operations

CryoSat-2
Sentinel-3

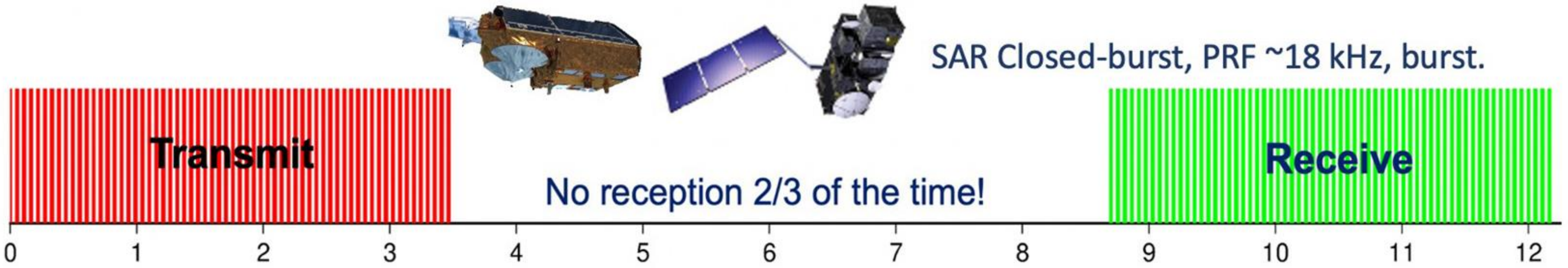

Sentinel-6 MF

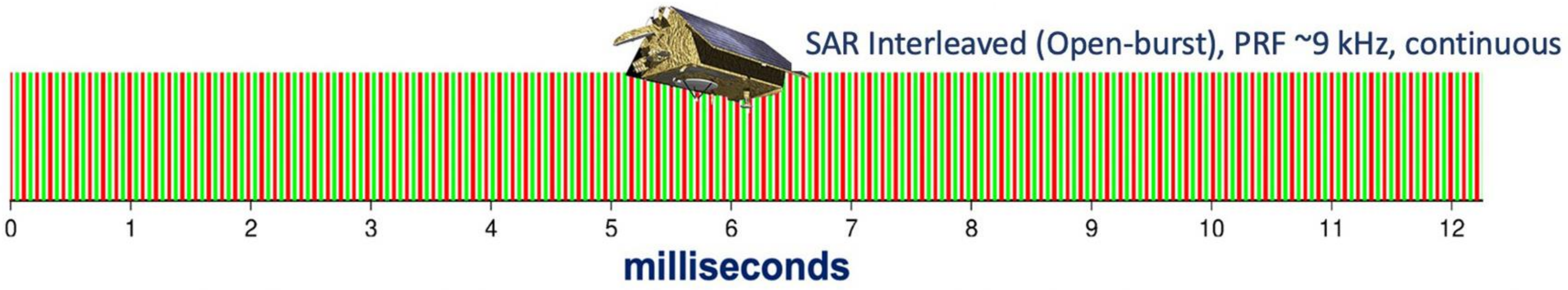

Donlon et al. (2021), doi.org/10.1016/j.rse.2021.112395

Synthetic aperture and along-track resolution

Here, a toy model of how measurement gaps cause frequency duplicates (grating lobes)

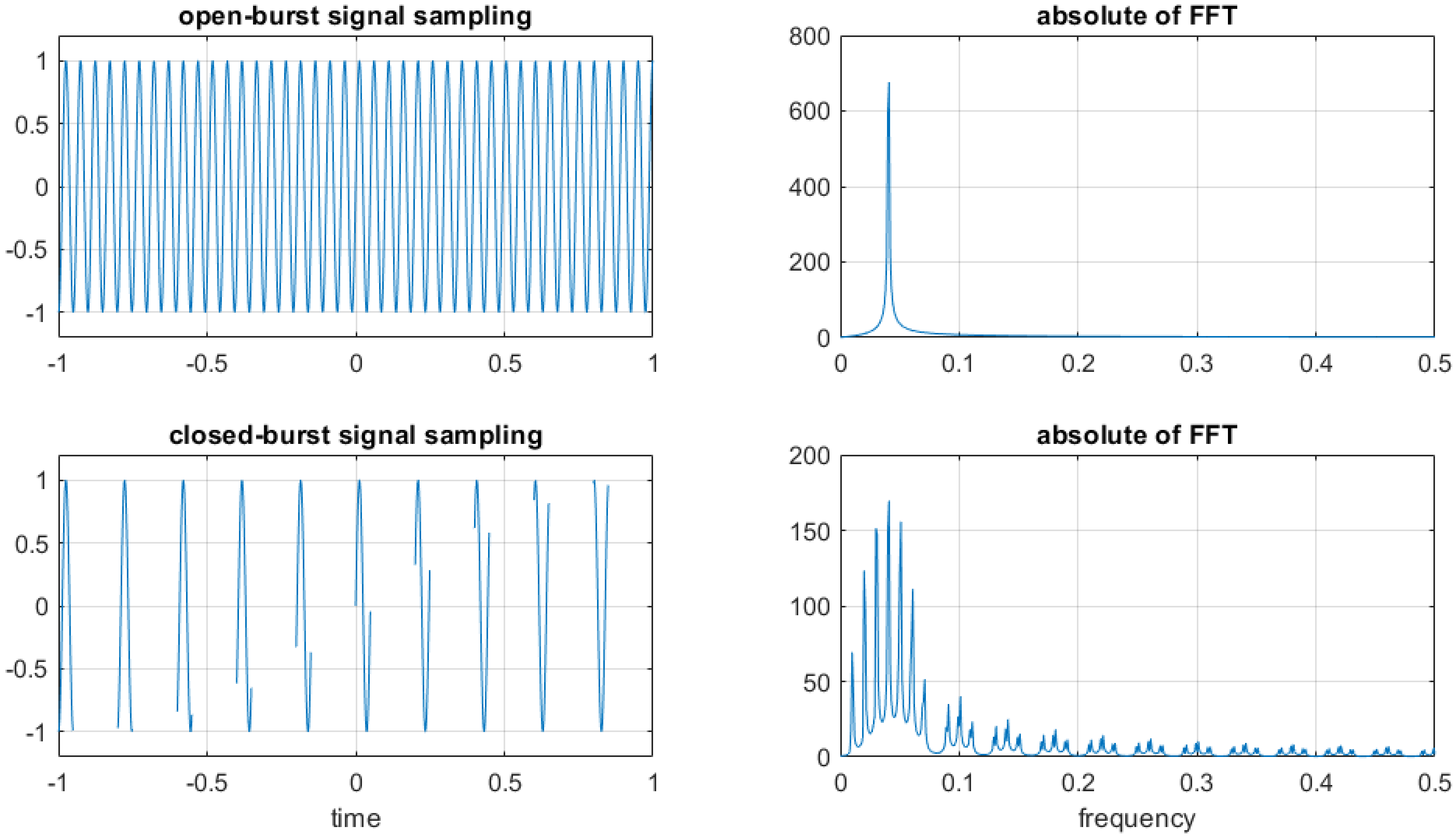

$$h^2_{\mathrm{FF}}(r,x) = h^2_{\mathrm{FF}}(r)h^2_{\mathrm{FF}}(x) \approx C\, \underbrace{\mathrm{sinc}^2\left[\frac{2B}{c}r\right]}_{\substack{\text{range sinc with}\\ \text{chirp resolution}}}\ \underbrace{\mathrm{sinc}^2\left[\frac{2T_b f_c V}{Hc}x\right]}_{\substack{\text{azimuth sinc with}\\ \text{UF-SAR resolution}}}\ \underbrace{\sum_n \mathrm{sinc}^2\left[T\frac{2f_cV}{Hc}\left(x - \overbrace{n\frac{Hc\mathrm{BRF}}{2f_cV}}^{\text{target copy positions}}\right)\right]}_{\substack{\text{repeated azimuth sincs with}\\ \text{FF-SAR resolution}}},$$

$$W_c(r) \approx C\int \mathrm{d}z\ p(z) \int \mathrm{d}y \int \mathrm{d}x\ \frac{G^2(x,y)\sigma_0(x,y)}{r^4} h_c^2(r - R(x,y,z),x), \quad (5)$$

$$W^{\mathrm{multi}}_{\mathrm{UF}}(r) = \sum_{t_b} W_{\mathrm{UF}}(r) \approx C\int \mathrm{d}z\ p(z) \int \mathrm{d}y\ G_y^2(y) \int \mathrm{d}x\ \underbrace{\sum_{t_b} G_x^2(x) h^2_{\mathrm{UF}}(r - R(x,y,z), x; x_l = Vt_b)}_{=I_{\mathrm{UF}}(x,y,z)},$$

$$I_{\mathrm{UF}}(x,y,z) \to \mathrm{sinc}^2\left[\frac{x}{L_x}\right]\sum_{t_b} G_x^2(Vt_b + x)\ \mathrm{sinc}^2\left[\frac{2B}{c}\left(r - r_0(y,z) - \left(\frac{xV}{H}t_b + \frac{x^2}{2H} - \frac{xf_cV}{Hs}\right)\right)\right] = \mathcal{T}_{\mathrm{UF}}(r - r_0, x),$$

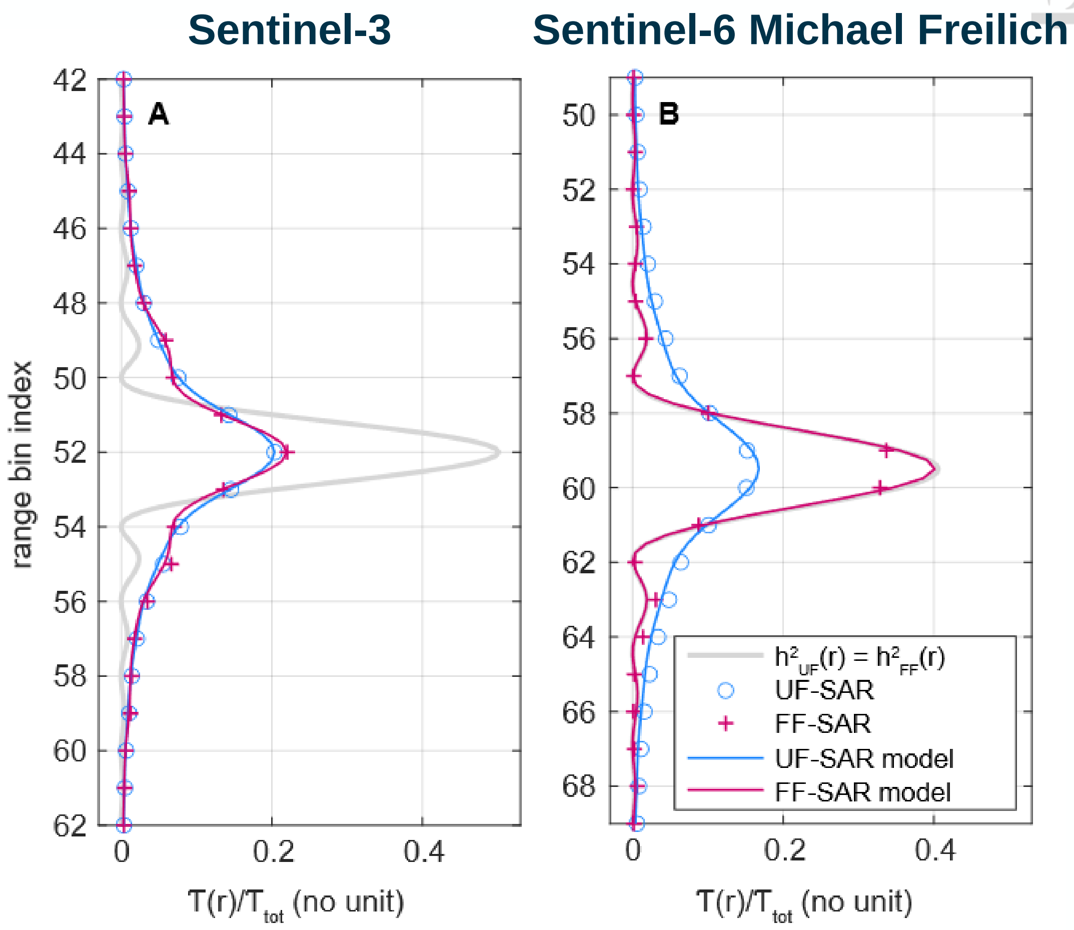

Fig. 10. Comparison of transponder images from Figs. 4 and 6 with IRF models from Eqs. 8 and 13 in terms of the flat line response $\mathcal{T}(r - r_0)$ for Sentinel-3 (panel A) and Sentinel-6 (panel B). The range offset r_0 was manually adjusted to represent the data best. Differences between UF-SAR and FF-SAR ocean waveforms are entirely governed by differences between these functions, when sea surface motion is neglected. The legend regards both panels.

Synthetic aperture and along-track resolution - Theory

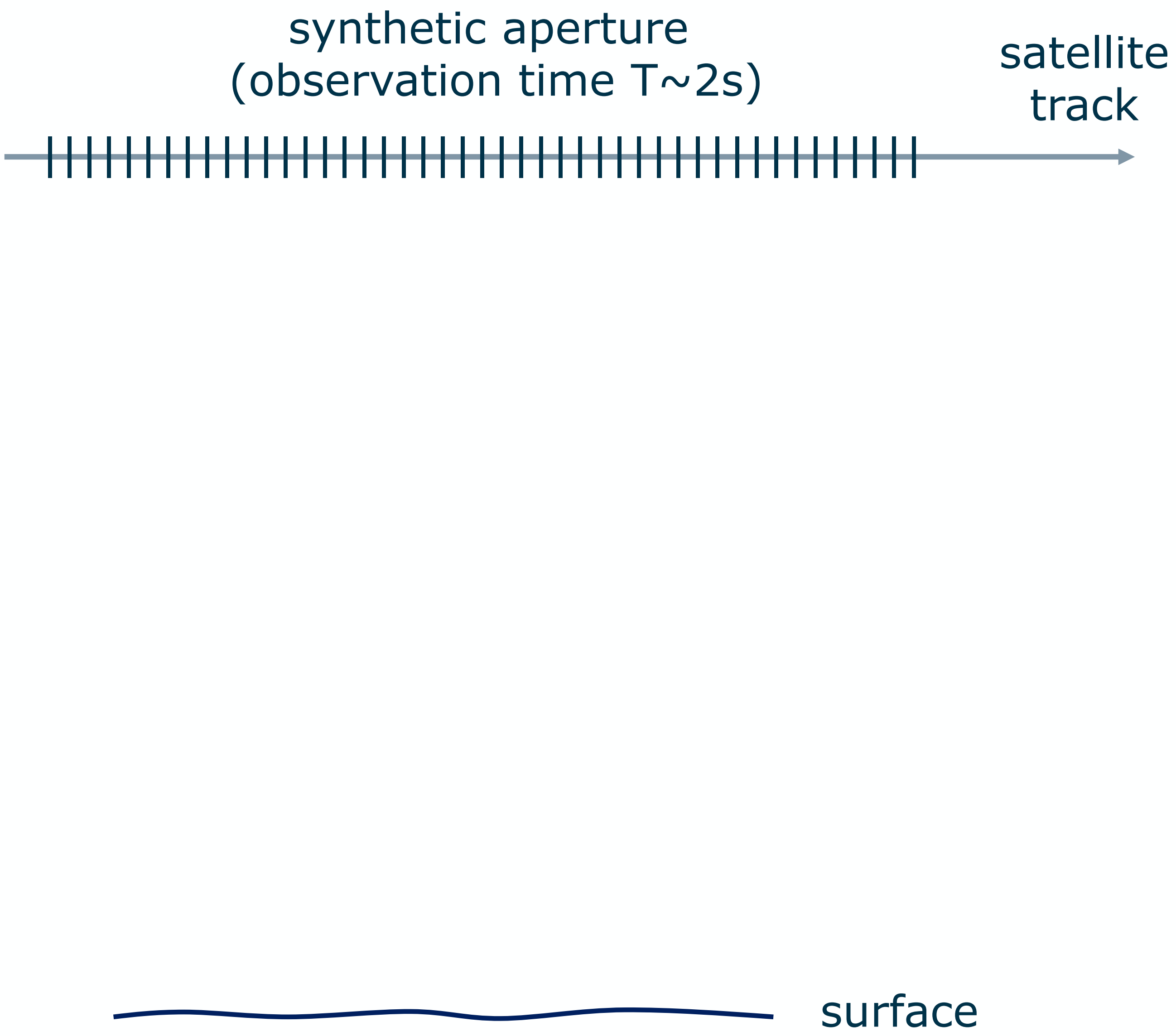

Synthetic aperture and along-track resolution - Theory

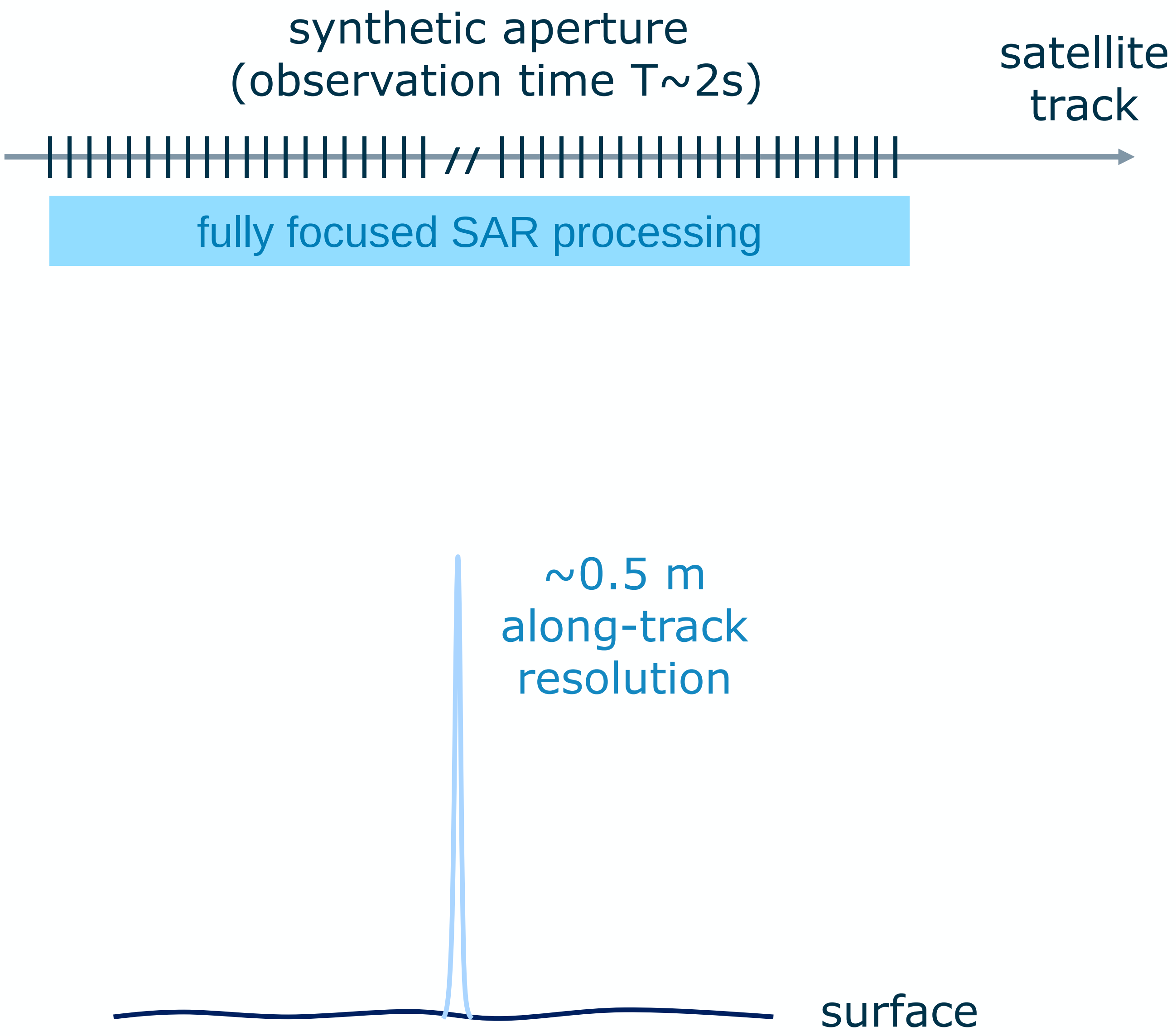

We can do the focusing over the whole aperture T. As in the FFT, the frequency resolution is then proportional to 1/T, about ~0.5 m along track distance for S3.

Synthetic aperture and along-track resolution - Theory

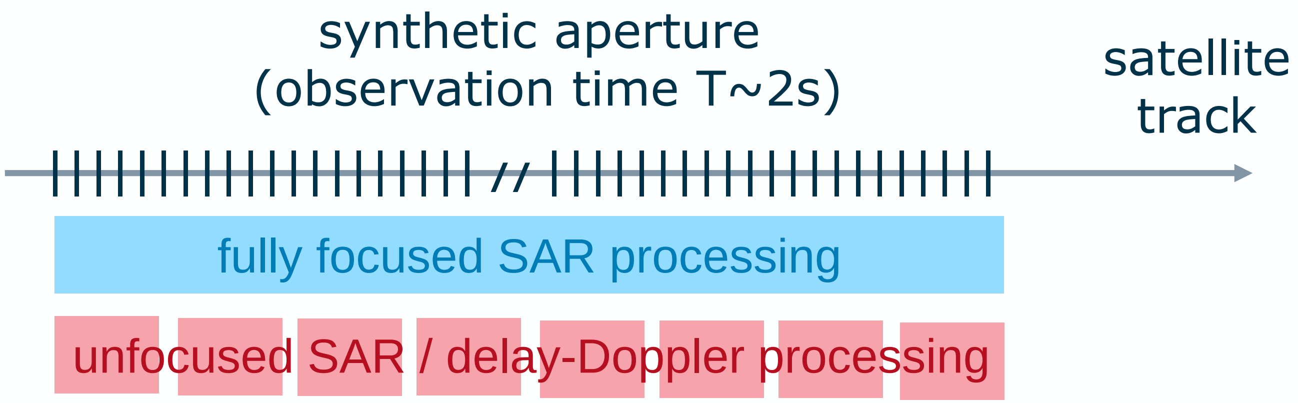

We can do the focusing over the whole aperture T. As in the FFT, the frequency resolution is then proportional to 1/T, about ~0.5 m along track distance for S3.

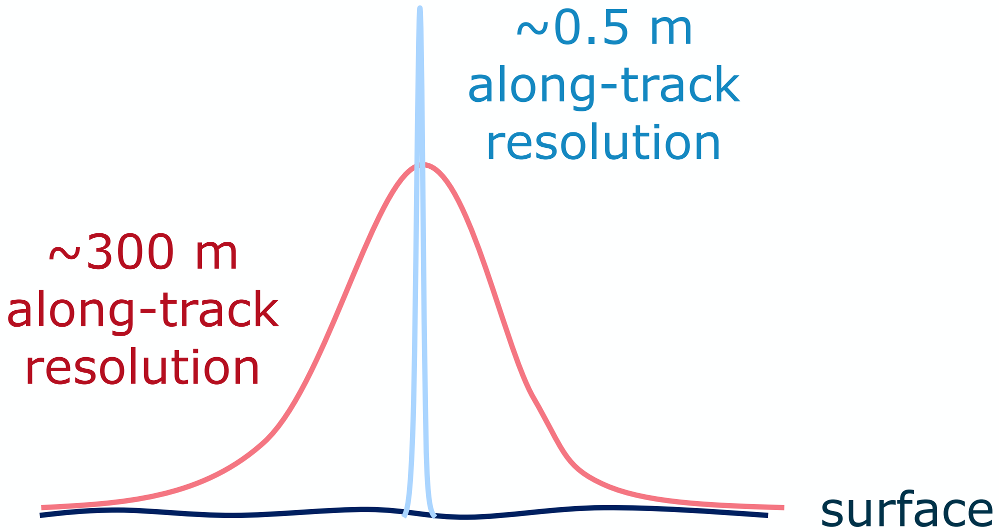

However, we can also subdivide the pulses into N chunks beforehand and on each perform the FFT, which is then averaged. The frequency resolution is then proportional to 1/(NT), about ~300 m along track distance for single S3 bursts with duration ~3.5 ms.

Egido et al. (2017), 10.1109/TGRS.2016.2607122

Synthetic aperture and along-track resolution

Sentinel-6 Michael Freilich

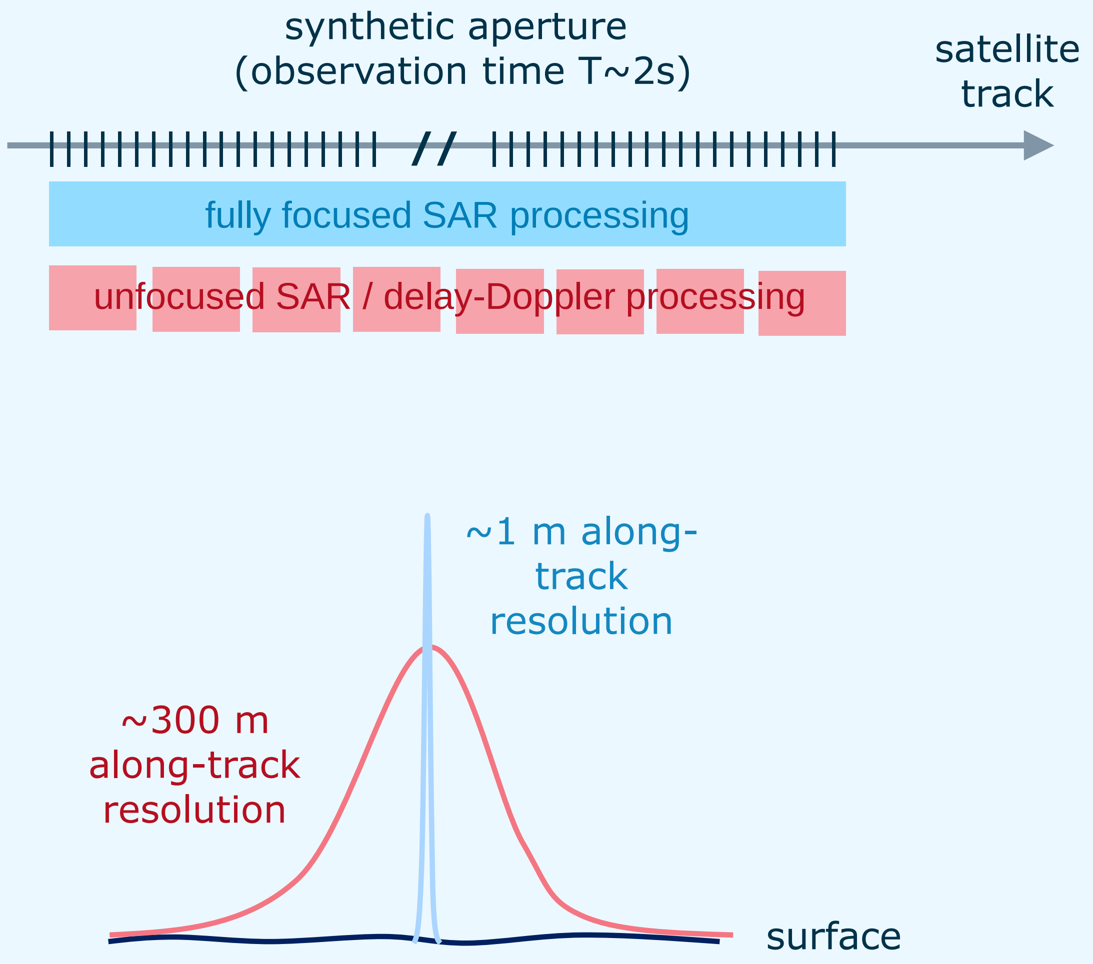

CryoSat-2 & Sentinel-3